The International Journal of Advanced Manufacturing Technology (2019) 101:1125–1132
https://doi.org/10.1007/s00170-018-2990-x

ORIGINAL ARTICLE

Interface characteristics of Mg/Al bimetal produced by a novel liquid-liquid compound casting process with an Al interlayer

Qiang Hu[1] · Zailiang Jiang[1] · Wenming Jiang[1] · Guangyu Li[1] · Feng Guan[1] · Haixiao Jiang[1] · Zitian Fan[1]

Received: 27 April 2018 / Accepted: 4 November 2018 / Published online: 14 November 2018

Abstract

Mg/Al bimetal was successfully prepared using a novel lost-foam casting (LFC) liquid-liquid compound process with an Al interlayer, and the interface characteristics including microstructure, mechanical properties, and fracture behavior of the Mg/Al bimetal were investigated in this paper. The results show that the mixing of AZ91D and A356 liquid metals was fully avoided by using the Al interlayer. A metallurgical bonding between the AZ91D alloy matrix and the A356 alloy matrix was achieved, obtaining a compact interface. The interface was constituted by the $Al_{12}Mg_{17} + \delta$ (Mg) eutectic and the Al_3Mg_2 and Mg_2Si reaction layers, which were respectively next to the AZ91D alloy matrix and the A356 alloy matrix. The reaction layers had much higher microhardnesses compared with the microhardnesses of the matrixes, and the highest microhardness up to 275–299 HV was obtained in the reaction layer next to the Al matrix. A brittle fracture morphology was observed in the fractured surface of the Mg/Al bimetal, and the fracture mainly initiated with the fracture of the reaction layer close to the Al matrix.

Keywords Mg/Al bimetal · Compound casting · Interlayer · Interface · Microstructure · Mechanical properties

1 Introduction

Mg/Al bimetals have a great potential in automobile and aerospace industrial applications, because they can simultaneously offer different expected properties of the magnesium and aluminum alloys [1–4]. However, the aluminum alloy is prone to forming an oxide film on its surface [5, 6], and the oxide film significantly increases the difficulty of the bonding between the magnesium and aluminum alloys. How to achieve a superior bonding of the magnesium alloy and the aluminum alloy is always an important subject. Currently, a large number of approaches have been developed to manufacture the Mg/Al bimetal, including compound casting [7–10], welding [11–15], extruding [16, 17], and rolling [18, 19], etc. Therein, the liquid-liquid compound casting method is considered as a simple and high-efficiency method for producing the Mg/Al bimetal without a solid insert. It should be noted that how to prevent different liquid metals from directly mixing is a challenging concept during the liquid-liquid compound casting process. Many researchers usually set an interlayer to avoid the mixing of different liquid metals [20–22].

Lost-foam casting (LFC) is a precision casting process, and it is suitable to fabricate complicated castings [23–26]. At present, the LFC process has become an attractive method to prepare bimetals combining its advantages, including no cores, complex geometries, smooth surface, and low cost [27, 28], etc. What is more, another attractive advantage for the LFC process is that the decomposition product of the foam pattern contains a plenty of reductive gas during the LFC process, which can protect the aluminum and magnesium alloys from oxidation [3, 9]. Some attempts have been performed to produce the Mg/Al bimetal using the liquid-solid compound method of the LFC technology [29, 30]. However, using the liquid-liquid compound method of the LFC technology to fabricate of the Mg/Al bimetal is always an unexplored field.

The Mg/Al bimetal was first produced using the liquid-liquid compound method of the LFC technology with an Al interlayer in this work, and the interlayer was used to avoid the mixing of different liquid metals. The objective of this work is to develop a new method to fabricate the Mg/Al bimetal. The interface characteristics including microstructure, mechanical

✉ Wenming Jiang
wmjiang@hust.edu.cn; jwenming@163.com

[1] State Key Lab of Materials Processing and Die & Mould Technology, Huazhong University of Science and Technology, Wuhan 430074, People's Republic of China

Table 1 Chemical compositions of the A356 and AZ91D alloys (wt%)

	Mass fraction						
Element	Si	Ti	Fe	Mn	Zn	Mg	Al
A356	6.81	0.017	0.205	–	–	0.439	Bal.
AZ91D	–	–	–	0.23	0.62	Bal.	9.08

properties as well as fracture behavior of the Mg/Al bimetal obtained using this new method were systematically investigated. In addition, the formation of the interface of the bimetal was also discussed.

2 Experimental procedure

The alloys materials including AZ91D magnesium and A356 aluminum alloys were chosen to prepare the Mg/Al bimetal in this work, and Table 1 lists the compositions of the alloys. A pure Al interlayer was used to avoid the mixing of the Mg and Al melts, which had a 2-mm thickness. The expanded polystyrene (EPS) material was used to fabricate foam patterns. The surface of the pure Al interlayer was first treated using grinding method with abrasive papers, and the Al interlayer was then degreased in an ethanol solution by an ultrasonic treatment for 15 min. Subsequently, the Al interlayer was quickly mounted into the foam pattern, and they were then dipped into a special refractory slurry to form a coating on the surface of the foam pattern, followed by drying inside an oven with a temperature of 50 °C holding for 2 h. Next, the modeling and compacting were performed, waiting for pouring process.

The Mg alloy and Al alloy ingots were melted by using resistance furnaces. The CO_2–0.5% SF_6 gas and the argon gas were respectively used as a protective gas atmosphere for the melt of the Mg and the refinement of the Al melt. When the temperatures of the Mg and Al melts reached 730 °C, the skimming of dross was performed. Subsequently, the Mg and Al melts with a temperature of 730 °C were poured into the foam patterns. Before pouring, the vacuum pump was opened to obtain a vacuum pressure of 0.03 MPa, thereby obtaining the Mg/Al bimetal when the liquid metal solidified. A schematic illustration of the novel compound casting setup used in this work is displayed in Fig. 1.

The sampling of the metallographic tests were conducted with a cutting machine in order to investigate the microstructure of the Mg/Al bimetal, and the metallographic samples were then ground using silicon carbide papers up to an average diameter of the grit of about 16.9 μm, and polished using an Al_2O_3 polishing solution, followed by etching with a 4% nital solution. The microstructure of the Mg/Al bimetal was observed using a DMM-490C metallographic microscope. A scanning electron microscope (SEM) was also employed to observe the microstructure of the Mg/Al bimetal. An energy-dispersive X-ray spectroscopy (EDS) attached to the SEM was used to analyze the phase constitutes of the interface of the Mg/Al bimetal. What is more, an X-ray diffraction (XRD) analysis was performed to analyze the phase constitutions of the interface.

The bonding strength of the Mg/Al bimetal was obtained via push-out tests [31, 32], and the push-out tests were performed by using a ZwickZ100 universal testing machine. The sizes of the push-out samples were 65 × 35 × 10 mm. A schematic illustration of the testing of the bonding strength is illustrated in Fig. 2. The Mg/Al push-out samples were pushed at a cross-head displacement rate of 0.5 mm/min to separate the Al alloy and the Mg alloy, thereby obtaining a maximum load. Then, the shear strength of the Mg/Al bimetal was calculated in term of the following equation [10].

$$\tau = {}^{F_{\max}}/_{A} \tag{1}$$

where τ, $F_{\max}$, and A present the shear strength, maximum load as well as the contact area of the bonding interface, respectively. The SEM and EDS analyzes were used to investigate the fracture behavior of the Mg/Al bimetal.

Furthermore, an HV-1000 hardness test instrument was employed to investigate microhardnesses of the interface of the Mg/Al bimetal with a load of 300 g and a holding time of 10 s.

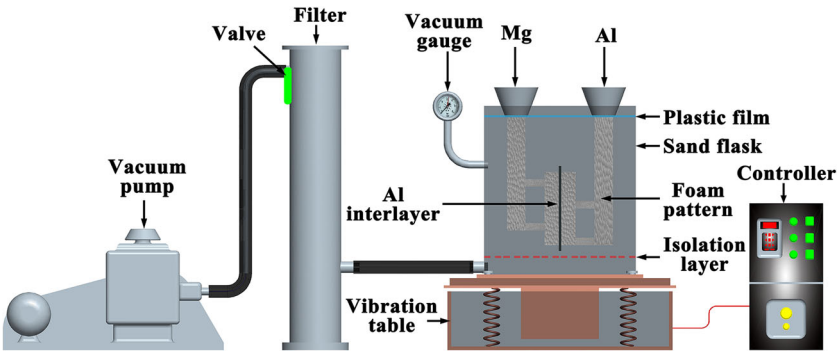

Fig. 1 Schematic illustration of the novel compound casting setup

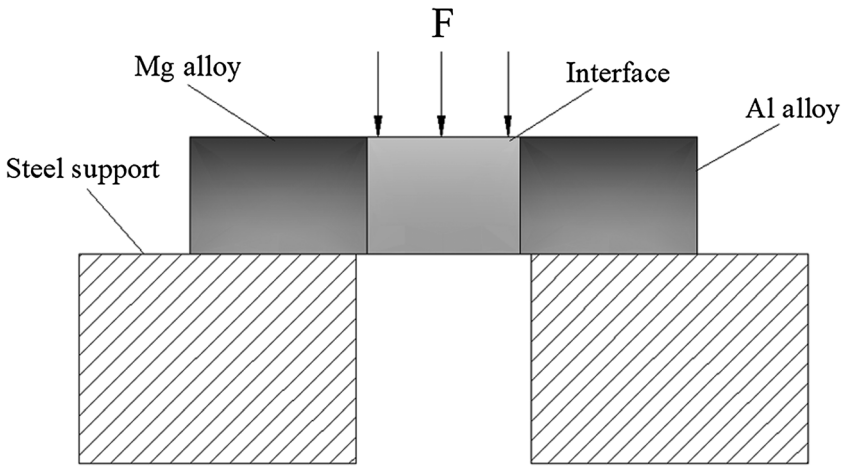

Fig. 2 Schematic illustration of the testing of the bonding strength

3 Results

3.1 Microstructure and phase composition

Figure 3 shows the optical micrographs of the interface of the Mg/Al bimetal. It is clear that an interface is observed between the Mg alloy and the Al alloy, exhibiting a compact morphology. The interface has a superior bonding with both the Mg matrix and the Al matrix. Moreover, it can be found that the interface of the Mg/Al bimetal is constituted by two reaction layers. Amidst the reaction, layers near to the Mg matrix and the Al matrix are named as the reaction layer I and the reaction layer II, respectively. They exhibit different morphologies and have a superior bonding (as shown in Fig. 3c).

More observations and component analysis of the interface were also performed in this study. The SEM micrographs of the interface are shown in Fig. 4, and the results of the EDS analysis at the interface are listed in Table 2. It is evident that the interface that includes the reaction layer I and the reaction layer II is very compact without obvious defects. In light of the EDS analysis results as well as the Al-Mg binary phase diagram [9, 33, 34], it can be inferred that the reaction layer I close to the Mg matrix is mainly constituted by the $Al_{12}Mg_{17} + \delta$ (Mg) eutectic. Therein, the $Al_{12}Mg_{17}$ phase has a successive distribution, and the δ (Mg) exhibits a dispersed morphology, as shown in Fig. 4a-a2. The reaction layer II near to the Al matrix primarily consists of the successive Al_3Mg_2 phase and dispersed Mg_2Si phase, and the Al_3Mg_2 phase occupies a main constituent in the reaction layer II (as shown in Fig. 4b2, c, c1, c2). In a word, the interface of the Mg/Al bimetal is constituted by the $Al_{12}Mg_{17} + \delta$ (Mg) eutectic, Al_3Mg_2 and Mg_2Si phases, and the $Al_{12}Mg_{17}$ and Al_3Mg_2 phases are the primary constituents at the interface, which is consistent with other reporters [7, 35].

The EDS mappings of the interface of the Mg/Al bimetal are shown in Fig. 5. It is evident that the Al and Mg elements have concentrations in the reaction layer I (as shown in Fig. 5a, a1, a2, b, b1, b2). Meanwhile, the concentrations of the Al, Mg, and Si elements are also obviously observed in the reaction layer II (as shown in Fig. 5b, b1, b2, b3, c, c1, c2, c3. The contents of the Mg and Al are basically stable at the

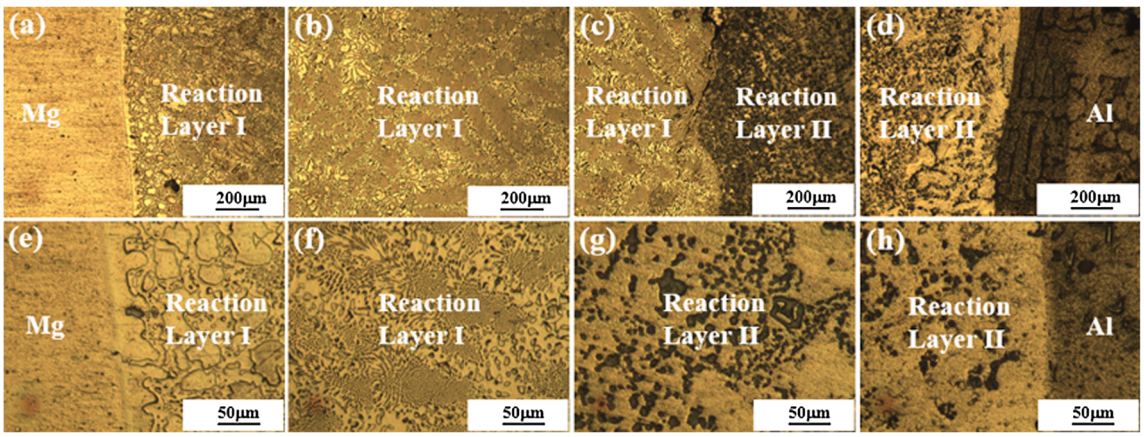

Fig. 3 Optical micrographs of the interface of the Mg/Al bimetal obtained by the novel compound casting. a, b, c, d Low magnification. e, f, g, h High magnification

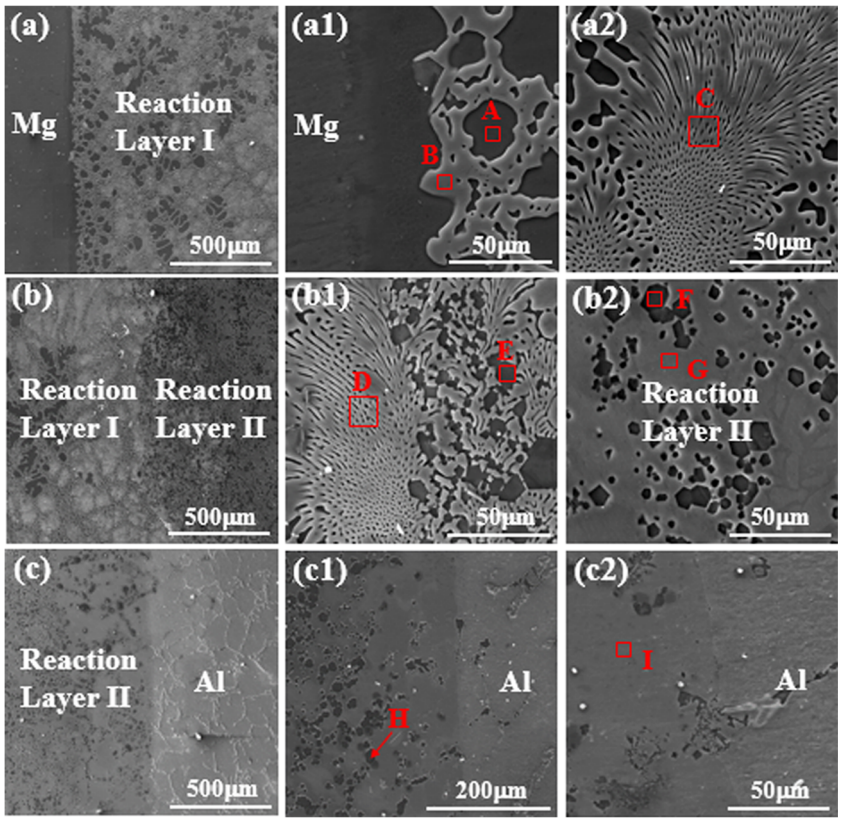

Fig. 4 SEM micrographs of the interface of the Mg/Al bimetal obtained by the novel compound casting. (a, a1, a2) Reaction layer I. (b, b1, b2) Intermediate layer. (c, c1, c2) Reaction layer II

interface. However, the content of the Si element is relatively less, and it mainly distributes in the reaction layer II. The results of the EDS mappings of the interface of the Mg/Al bimetal imply that a superior metallurgical interface has generated between two matrixes.

In addition, the further confirmation of the constitutive phases at the interface was also performed using the XRD analysis method, as shown in Fig. 6. The result of the XRD analysis also suggests that the $Al_{12}Mg_{17} + \delta$ (Mg) eutectic, Al_3Mg_2 as well as Mg_2Si are the main constitutive phases of the interface of the Mg/Al bimetal.

3.2 Mechanical properties

Figure 7 shows the results of the microhardness testing of the Mg/Al bimetal. The results of the microhardness indicate that the reaction layers of the Mg/Al bimetal have significantly higher microhardnesses in comparison with the matrixes. The reaction layer I next to the Mg matrix obtains the microhardness of about 135–220 HV, which is attributed to the existence of the $Al_{12}Mg_{17} + \delta$ (Mg) eutectic. The reaction layer II close to the Al matrix has the microhardness of 275–299 HV, exhibiting that the Al_3Mg_2

Table 2 The results of the EDS analysis of the interface

Area no.	Element compositions (at%)			Element compositions ratio (Al/Mg)	Element compositions ratio (Mg/Si)	Inferred compound
	Al	Mg	Si			
A	11.25	88.75	–	0.13	–	δ-Mg
B	38.22	61.78	–	0.62	–	$Al_{12}Mg_{17}$
C	34.26	65.74	–	0.52	–	$Al_{12}Mg_{17} + \delta$-Mg
D	34.71	65.29	–	0.53	–	$Al_{12}Mg_{17} + \delta$-Mg
E	–	64.20	35.80	–	1.79	Mg_2Si
F	–	59.86	40.14	–	1.49	Mg_2Si
G	59.13	40.87	–	1.45	–	Al_3Mg_2
H	–	59.11	40.89	–	1.45	Mg_2Si
I	62.67	37.33	–	1.68	–	Al_3Mg_2

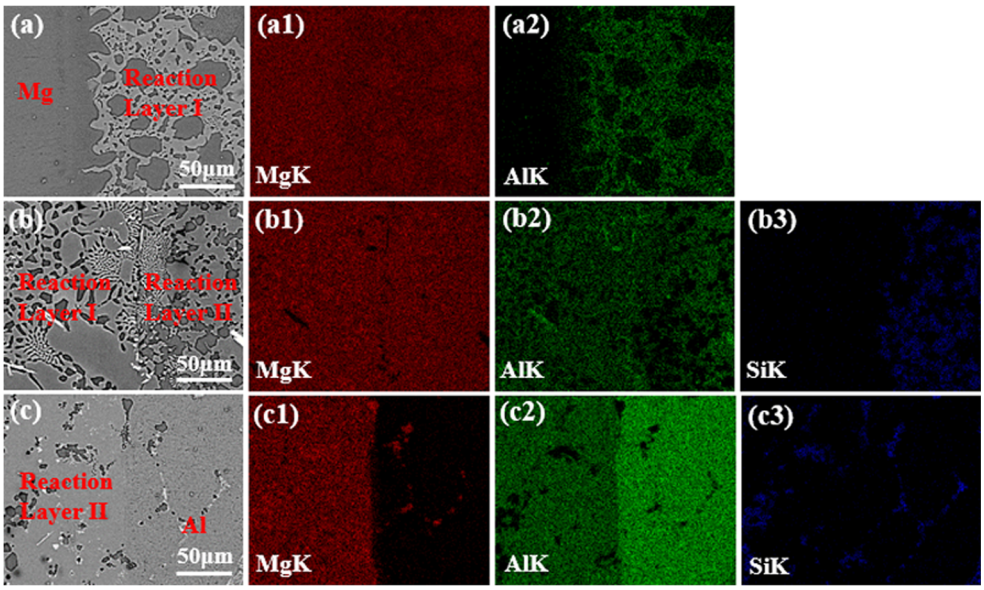

Fig. 5 SEM micrographs and EDS mappings of the Mg/Al bimetal obtained by the novel compound casting. (a, a1, a2) Reaction layer I. (b, b1, b2, b3) Intermediate layer. (c, c1, c2, c3) Reaction layer II

intermetallic phase obtains the highest microhardness at the interface, while the microhardnesses are 38–50 and 63–81 HV for the Mg matrix and the Al matrix, respectively. The results of the microhardness testing suggest that a metallurgical interface has formed between two matrixes, and the $Al_{12}Mg_{17}$ and Al_3Mg_2 intermetallic compounds belong to hard phases, especially in the Al_3Mg_2 intermetallic phase [36, 37]. A larger number of the hard intermetallic phases at the interface will weaken the bonding strength of the bimetal [38].

In addition, the shear strength of the Mg/Al bimetal is obtained through the push-out testing, and it is about 9.14 MPa. In the future, our investigations will focus on the further improvement of the shear strength of the Mg/Al bimetal. Figure 8 exhibits the SEM fractographs and EDS analysis of the Mg/Al bimetal. It is obvious that a brittle fracture nature is found in the fractographs of the Mg/Al bimetal, and some flat planes are observed in the fractured surface (as shown in Fig. 8a). The EDS results indicate that the fracture of the Mg/Al bimetal mainly occurs in the Al_3Mg_2 intermetallic phase (as shown in Fig. 8b, c). It can be explained by the fact that the Al_3Mg_2 phase occupies a significant proportion at the interface; at the same time, it has the highest microhardness at the interface of the Mg/Al bimetal (as shown in Fig. 7). In this case, the Al_3Mg_2 hard phase becomes a main stress concentration source, thereby easily cracking when it is subjected to an applied load [39, 40]. Moreover, the Mg_2Si particle is also detected at the fractured surface of the Mg/Al bimetal (as shown in Fig. 8d). Therefore, it reveals that the fracture of the Mg/Al bimetal mainly occurs in the reaction layer close to the Al matrix.

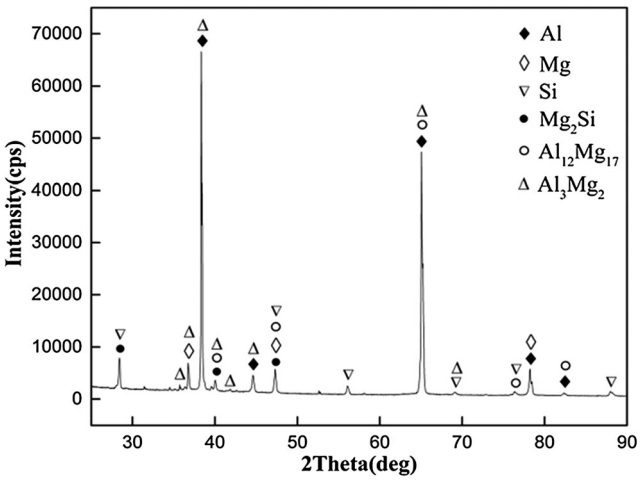

Fig. 6 XRD patterns of the phases at the interface of the Mg/Al bimetal obtained by the novel compound casting

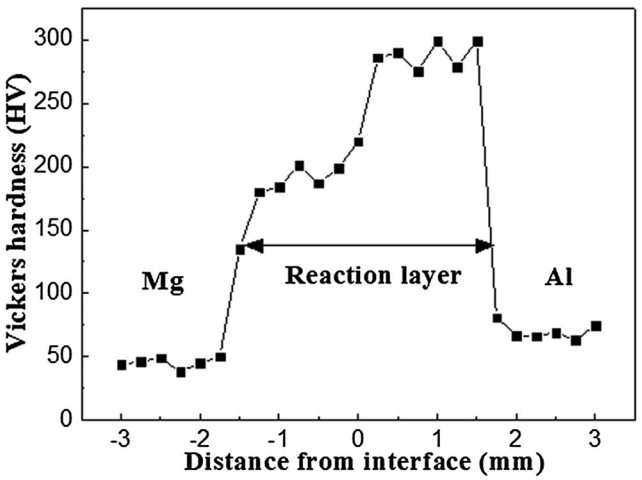

Fig. 7 Microhardness results of the Mg/Al bimetal obtained by the novel compound casting

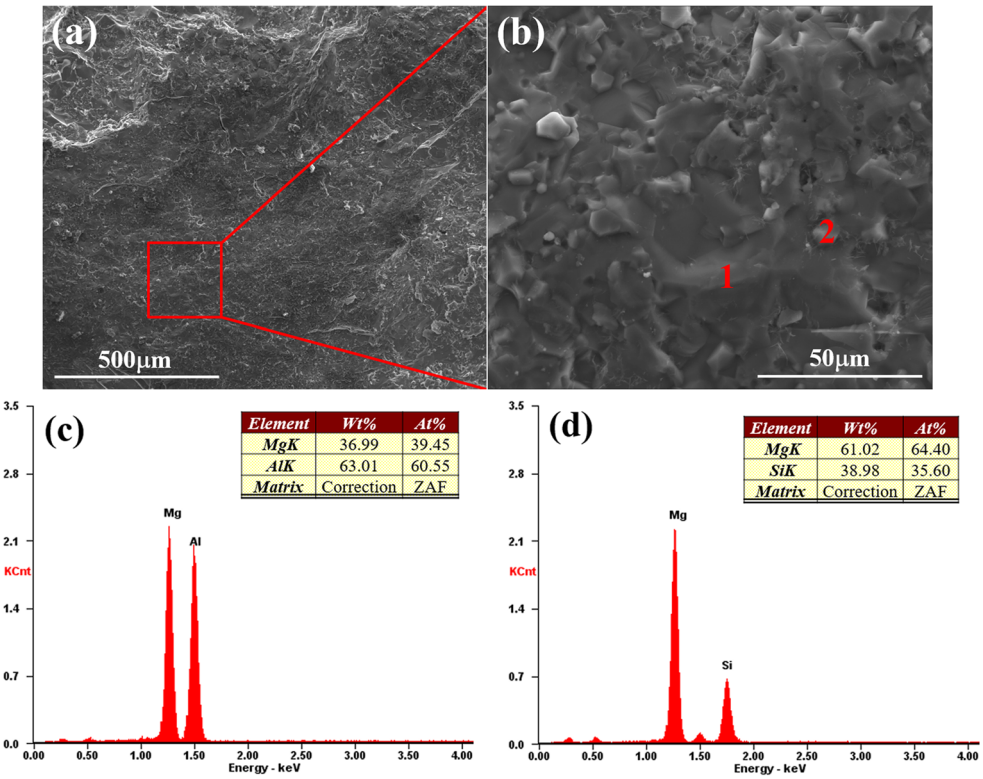

Fig. 8 SEM fractographs and EDS analysis of the fractured surface of the Mg/Al bimetal. (a) Low magnification SEM fractograph. (b) High magnification SEM fractograph. (c, d) EDS analysis results corresponding to areas 1 and 2 indicated in (b), respectively

4 Discussion

Figure 9 shows a schematic illustration of the formation process of the interface. First, the Mg and Al melts quickly fill with the foam mold under a negative pressure. When the Mg and Al melts meet with the foam patterns, the decomposition of the foam patterns rapidly occurs, as shown in Fig. 9a. With the further filling of the Mg and Al melts, the Al interlayer is gradually melted when the Mg and Al melts contact with the Al interlayer, because the pouring temperatures of the Mg and Al alloys are higher than the melting temperature of the Al in this work. The Al element from the Al interlayer then diffuses into the Mg and Al melts; meanwhile, the Mg, Al, and Si elements from the matrixes also continuously interdiffuse, forming a partial mixing molten pool of the Mg alloy melt, Al alloy melt with the pure Al melt (as shown in Fig. 9b. The interdiffusion among different elements results in the concentration gradient of the Al, Mg, and Si elements, and the metallurgical reaction occurs among the Al, Mg, and Si elements (as shown in Fig. 9c). With the decrease of the melt temperature, the $Al_{12}Mg_{17} + \delta$ (Mg) eutectic forms close to the Mg matrix through the following reaction: $L \rightarrow Al_{12}Mg_{17} + \delta$ eutectic transformation at 437 °C [7, 9]. Near to the Al alloy melt, the Al_3Mg_2 phase next to the Al matrix forms because of high content of the Al. For the Mg_2Si phase, its formation is mainly attributed to the reaction of the Mg and Si respectively from the Mg alloy melt and the Al alloy melt. After solidified, the Mg/Al bimetal with a metallurgical interface is obtained (as shown in Fig. 9d). Consequently, a comprehensive mechanism of the fusion bonding and diffusion bonding is responsible for the formation of the interface of the Mg/Al bimetal during the novel compound casting.

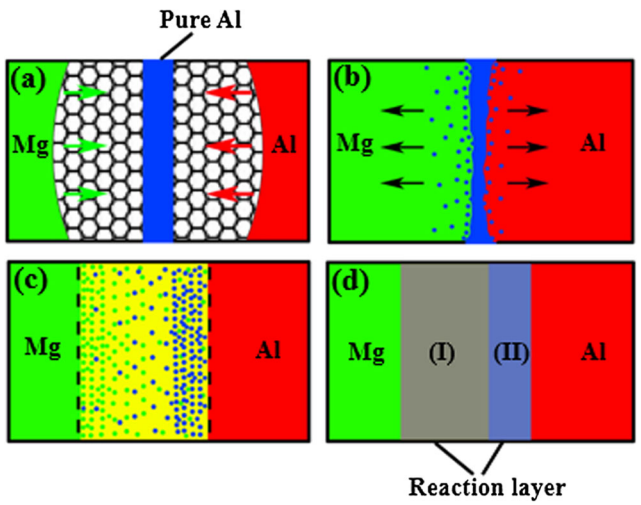

Fig. 9 Schematic illustration of the formation of the interface of the Mg/Al bimetal obtained by the novel compound casting. (a) Filling of the melts. (b) Melting of the interlayer and diffusing of different elements. (c) Reacting among different elements. (d) Forming of the interface

5 Conclusion

(1) The Mg/Al bimetal was produced by the novel compound casting method together with the Al interlayer. The mixing of the AZ91D and A356 liquid metals was fully avoided by using the Al interlayer. A metallurgical bonding between the AZ91D alloy matrix and the A356 alloy matrix was achieved, obtaining a compact interface.

(2) The interface of the Mg/Al bimetal was constituted by the $Al_{12}Mg_{17} + \delta$ (Mg) eutectic and the Al_3Mg_2 and Mg_2Si reaction layers, which were respectively next to the AZ91D alloy matrix and the A356 alloy matrix. The comprehensive mechanism of the fusion bonding and diffusion bonding was responsible for the formation of the interface of the Mg/Al bimetal.

(3) The reaction layers had much higher microhardnesses compared with the microhardnesses of the Mg and Al matrixes. The reaction layer next to the Mg matrix obtained the microhardness of about 135–220 HV, and the microhardness of the reaction layer next to the Al matrix was the highest microhardness at the interface, up to 275–299 HV.

(4) The Mg/Al bimetal obtained a shear strength of approximately 9.14 MPa. The fracture of the Mg/Al bimetal mainly occurred in the reaction layer close to the Al matrix, exhibiting a typical brittle fracture morphology.

Funding information This study is supported by the National Natural Science Foundation of China (Nos. 51775204 and 51204124), the fund of the State Key Laboratory of Solidification Processing in NWPU (No. SKLSP201821), the Natural Science Foundation of Hubei Province, China (No. 2017CFB488), and the Analytical and Testing Center, HUST.

References

1. Jiang WM, Chen X, Wang BJ, Fan ZT, Wu HB (2016) Effects of vibration frequency on microstructure, mechanical properties, and fracture behavior of A356 aluminum alloy obtained by expendable pattern shell casting. Int J Adv Manuf Technol 83(1–4):167–175. https://doi.org/10.1007/s00170-015-7586-0
2. Zhang H, Chen YQ, Luo AA (2014) A novel aluminum surface treatment for improved bonding in magnesium/aluminum bimetallic castings. Scr Mater 86:52–55. https://doi.org/10.1016/j.scriptamat.2014.05.007
3. Li GY, Jiang WM, Fan ZT, Jiang ZL, Liu XW, Liu FC (2017) Effects of pouring temperature on microstructure, mechanical properties, and fracture behavior of Al/Mg bimetallic composites produced by lost foam casting process. Int J Adv Manuf Technol 91(1–4):1355–1368. https://doi.org/10.1007/s00170-016-9810-y
4. Kund NK (2018) Effect of tilted plate vibration on solidification and microstructural and mechanical properties of semisolid cast and heat-treated A356 Al alloy. Int J Adv Manuf Technol 97(5–8):1617–1626. https://doi.org/10.1007/s00170-018-2063-1
5. Campbell J (2011) Complete casting handbook, first edn. Elsevier Press, UK
6. Campbell J (2006) Entrainment defects. Mater Sci Technol 22(2):127–145. https://doi.org/10.1179/174328406X74248
7. Hajjari E, Divandari M, Razavi SH, Homma T, Kamado S (2012) Microstructure characteristics and mechanical properties of Al 413/Mg joint in compound casting process. Metall Mater Trans A 43(12):4667–4677. https://doi.org/10.1007/s11661-012-1296-0
8. Xu GC, Luo AA, Chen YQ, Sachdev AK (2014) Interfacial phenomena in magnesium/aluminum bi-metallic castings. Mater Sci Eng A 595:154–158. https://doi.org/10.1016/j.msea.2013.11.093
9. Jiang WM, Fan ZT, Li GY, Yang L, Liu XW (2016) Effects of melt-to-solid insert volume ratio on the microstructures and mechanical properties of Al/Mg bimetallic castings produced by lost foam casting. Metall Mater Trans A 47(12):6487–6497. https://doi.org/10.1007/s11661-016-3788-9
10. Liu JC, Hu J, Nie XY, Li HX, Du Q, Zhang JS, Zhuang LZ (2015) The interface bonding mechanism and related mechanical properties of Mg/Al compound materials fabricated by insert molding. Mater Sci Eng A 635:70–76. https://doi.org/10.1016/j.msea.2015.03.074
11. Islam MR, Ishak M, Shah LH, Idris SR, Meriç C (2016) Dissimilar welding of A7075-T651 and AZ31B alloys by gas metal arc plug welding method. Int J Adv Manuf Technol 88(9–12):2773–2783. https://doi.org/10.1007/s00170-016-8993-6
12. Tabasi M, Farahani M, Besharati Givi MK, Farzami M, Moharami A (2016) Dissimilar friction stir welding of 7075 aluminum alloy to AZ31 magnesium alloy using SiC nanoparticles. Int J Adv Manuf Technol 86(1–4):705–715. https://doi.org/10.1007/s00170-015-8211-y
13. Mofid MA, Abdollah-Zadeh A, Gür CH (2014) Investigating the formation of intermetallic compounds during friction stir welding of magnesium alloy to aluminum alloy in air and under liquid nitrogen. Int J Adv Manuf Technol 71(5–8):1493–1499. https://doi.org/10.1007/s00170-013-5565-x
14. Zhao Y, Jiang S, Yang SF, Lu ZP, Yan K (2016) Influence of cooling conditions on joint properties and microstructures of aluminum and magnesium dissimilar alloys by friction stir welding. Int J Adv Manuf Technol 83(1–4):673–679. https://doi.org/10.1007/s00170-015-7624-y
15. Manladan SM, Yusof F, Ramesh S, Fadzil M (2016) A review on resistance spot welding of magnesium alloys. Int J Adv Manuf Technol 86(5–8):1805–1825. https://doi.org/10.1007/s00170-015-8258-9
16. Feng B, Xin YC, Yu HH, Hong R, Liu Q (2016) Mechanical behavior of a Mg/Al composite rod containing a soft Mg sleeve and an ultra hard Al core. Mater Sci Eng A 675:204–211. https://doi.org/10.1016/j.msea.2016.08.069
17. Feng B, Xin YC, Guo FL, Yu HH, Wu Y, Liu Q (2016) Compressive mechanical behavior of Al/Mg composite rods with different types of Al sleeve. Acta Mater 120:379–390. https://doi.org/10.1016/j.actamat.2016.08.079
18. Zha M, Meng XT, Zhang HM, Zhang XH, Jia HL, Li YJ, Zhang JY, Wang HY, Jiang QC (2017) High strength and ductile high solid solution Al-Mg alloy processed by a novel hard-plate rolling route. J Alloys Compd 728:872–877. https://doi.org/10.1016/j.jallcom.2017.09.017
19. Gali OA, Shafiei M, Hunter JA, Riahi AR (2016) The initiation of roll coating buildup during thermomechanical processing of aluminum-magnesium alloys. Surf Coat Technol 308:328–336. https://doi.org/10.1016/j.surfcoat.2016.07.102
20. Dai XY, Zhang HT, Wang B, Ji A, Liu JH, Feng JC (2016) Improving weld strength of arc-assisted ultrasonic seam welded

Mg/Al joint with Sn interlayer. Mater Des 98:262–271. https://doi.org/10.1016/j.matdes.2016.02.095
21. Liu F, Zhang ZD, Liu LM (2012) Microstructure evolution of Al/Mg butt joints welded by gas tungsten arc with Zn filler metal. Mater Charact 69:84–89. https://doi.org/10.1016/j.matchar.2012.04.012
22. Zhang HT, Dai XY, Feng JC (2014) Joining of aluminum and magnesium via pre-roll-assisted A-TIG welding with Zn interlayer. Mater Lett 122:49–51. https://doi.org/10.1016/j.matlet.2014.02.008
23. Griffiths WD, Ainsworth MJ (2016) Instability of the liquid metal-pattern interface in the lost foam casting of aluminum alloys. Metall Mater Trans A 47:3137–3149. https://doi.org/10.1007/s11661-016-3461-3
24. Jiang WM, Fan ZT, Liu DJ, Liao DF, Zhao Z, Dong XP, Wu HB (2012) Influence of process parameters on filling ability of A356 aluminium alloy in expendable pattern shell casting with vacuum and low pressure. Int J Cast Metal Res 25(1):47–52. https://doi.org/10.1179/1743133611Y.0000000014
25. Charchi A, Rezaei M, Hossainpour S, Shayegh J, Falak S (2010) Numerical simulation of heat transfer and fluid flow of molten metal in MMA-St copolymer lost foam casting process. J Mater Process Technol 210(14):2071–2080. https://doi.org/10.1016/j.jmatprotec.2010.07.028
26. Jiang WM, Fan ZT, Liu DJ, Wu HB (2013) Influence of gas flowrate on filling ability and internal quality of A356 aluminum alloy castings fabricated using the expendable pattern shell casting with vacuum and low pressure. Int J Adv Manuf Technol 67(9–12):2459–2468. https://doi.org/10.1007/s00170-012-4663-5
27. Emami SM, Divandari M, Hajjari E, Arabi H (2013) Comparison between conventional and lost foam compound casting of Al/Mg light metals. Int J Cast Metal Res 26(1):43–50. https://doi.org/10.1179/1743133612Y.0000000037
28. Jiang WM, Fan ZT, Liu DJ (2012) Microstructure, tensile properties and fractography of A356 alloy under as-cast and T6 obtained with expendable pattern shell casting process. Trans Nonferrous Metals Soc China 22:S7–S13. https://doi.org/10.1016/S1003-6326(12)61676-8
29. Guler KA, Kisasoz A, Karaaslan A (2014) Fabrication of Al/Mg bimetal compound casting by lost foam technique and liquid-solid process. Mater Test 56(9):700–702. https://doi.org/10.3139/120.110624
30. Jiang WM, Li GY, Fan ZT, Wang L, Liu FC (2016) Investigation on the interface characteristics of Al/Mg bimetallic castings processed by lost foam casting. Metall Mater Trans A 47(5):2462–2470. https://doi.org/10.1007/s11661-016-3395-9
31. Dezellus O, Zhe M, Bosselet F, Rouby D, Viala JC (2011) Mechanical testing of titanium/aluminium-silicon interface. Effect of T6 heat treatment. Mater Sci Eng A 528(6):2795–2803. https://doi.org/10.1016/j.msea.2010.12.036
32. Jiang WM, Fan ZT, Li GY, Li C (2016) Effects of zinc coating on interfacial microstructures and mechanical properties of aluminum/steel bimetallic composites. J Alloys Compd 678:249–257. https://doi.org/10.1016/j.jallcom.2016.03.276
33. He K, Zhao JH, Li P, He JS, Tang Q (2016) Investigation on microstructures and properties of arc-sprayed-Al/AZ91D bimetallic material by solid-liquid compound casting. Mater Des 112:553–564. https://doi.org/10.1016/j.matdes.2016.09.085
34. Hajjari E, Divandari M, Razavi SH, Homma T, Kamado S (2012) Intermetallic compounds and antiphase domains in Al/Mg compound casting. Intermetallics 23:182–186. https://doi.org/10.1016/j.intermet.2011.12.001
35. Ren QS, Zhao CZ, Li ZB, Zhang HX (2015) Microstructure and mechanical properties of Mg/Al bimetallic composite fabricated by compound casting. Mater Res Innov 19:S73–S78. https://doi.org/10.1179/1432891715Z.0000000001520
36. Liu ZL, Ji SD, Meng XC (2018) Joining of magnesium and aluminum alloys via ultrasonic assisted friction stir welding at low temperature. Int J Adv Manuf Technol 97(9–12):4127–4136. https://doi.org/10.1007/s00170-018-2255-8
37. Shah LH, Gerlich A, Zhou Y (2018) Design guideline for intermetallic compound mitigation in Al-Mg dissimilar welding through addition of interlayer. Int J Adv Manuf Technol 94(5–8):2667–2678. https://doi.org/10.1007/s00170-017-1038-y
38. Jiang Z, Fan Z, Jiang W, Li G, Wu Y, Guan F, Jiang H (2018) Interfacial microstructures and mechanical properties of Mg/Al bimetal produced by a novel liquid-liquid compound casting process. J Mater Process Technol 261:149–158. https://doi.org/10.1016/j.jmatprotec.2018.06.013
39. Baqer YM, Ramesh S, Yusof F, Manladan SM (2018) Challenges and advances in laser welding of dissimilar light alloys: Al/Mg, Al/Ti, and Mg/Ti alloys. Int J Adv Manuf Technol 95(9–12):4353–4369. https://doi.org/10.1007/s00170-017-1565-6
40. Liu ZL, Ji SD, Meng XC, Huang RF (2017) Improving joint formation and tensile properties of friction stir welded ultra-thin Al/Mg alloy sheets using a pinless tool assisted by a stationary shoulder. Int J Adv Manuf Technol 93(5–8):2071–2079. https://doi.org/10.1007/s00170-017-0682-6